Check for updates

Benefits of Dual Wings over Single Wings for High-Performance Business Airplanes

Mark D. Rhodes* and Bruce P. Selberg†
University of Missouri, Rolla, Missouri

An investigation was performed to compare closely coupled dual-wing aircraft and swept-forward swept-rearward (SFSR), dual-wing aircraft to corresponding single-wing aircraft to judge the advantages offered by aircraft designed with multiple-wing systems. The optimum dual-wing geometry used on the dual-wing designs were determined in an analytical study which investigated the two- and three-dimensional aerodynamic behavior of a wide range of dual-wing configurations in order to find the wing geometry that created the minimum cruise drag. This analysis used a multielement inviscid vortex panel program coupled to a momentum integral boundary-layer analysis program to calculate the two-dimensional aerodynamic data, which was then used as input for a three-dimensional vortex-lattice program, which calculated the three-dimensional aerodynamic data. The low drag of the dual-wing configurations is due to a combination of two- and three-dimensional drag reductions, and the structural advantages of the two wings, which permitted higher aspect ratios for the two wing systems, because of the wing tip structural connections.

Downloaded by ISAE on October 25, 2021 | http://arc.aiaa.org | DOI: 10.2514/3.48234

Nomenclature

AR	= aspect ratio, b^2/S_{ref}
b	= wing span
C_D	= total drag coefficient
$C_{D_{cr}}$	= cruise drag coefficient
C_{D_i}	= induced drag coefficient
C_d	= sectional drag coefficient
C_L	= total lift coefficient
$C_{L_{cr}}$	= cruise lift coefficient
C_l	= sectional lift coefficient
C_l/C_d	= sectional lift-to-drag ratio
C_{l_α}	= sectional lift curve slope
C_p	= pressure coefficient, $(p-p_\infty)/q_\infty$
c	= wing chord
D	= decalage angle
D_{cr}	= cruise drag
G	= gap (in chord lengths)
L/D	= total lift-to-drag ratio
$(L/D)_{cr}$	= cruise lift-to-drag ratio
P_{cr}	= cruise power
R	= Reynolds number, per meter or foot
R_c	= Reynolds number based on wing chord
S	= stagger (in chord lengths)
V_{cr}	= cruise speed
W_{cr}	= cruise weight
x/c	= nondimensional chordwise location
α	= wing angle of attack
ΔD_i	= percent reduction in induced drag
λ	= taper ratio, c_{tip}/c_{root}

Introduction

WITH the advent of the all-metal aircraft wing, the biplane and triplane wing designs used on most of the early aircraft were replaced by a single-wing surface which was structurally stronger and aerodynamically "cleaner" than the multisurface wings it replaced. Progressively lighter and more powerful aircraft engines and higher flight speeds obviated the need for the additional wing area provided by the multisurface wings. However, more recent studies have shown that closely coupled dual-wing systems possess aerodynamic advantages over the single-wing configuration that could lead to dual-wing aircraft designs that are more fuel efficient than single-wing designs by virtue of the lower drag of the dual wings.

The three main factors affecting the performance of a closely coupled dual-wing system with the same airfoils and equal chords are stagger S, the longitudinal separation of the wings; gap G, the vertical distance between the wings; and decalage D, the relative angle between the two wings. Both stagger and gap are measured from midchord to midchord and nondimensionalized with respect to chord length c. Gap is always positive, stagger is positive when the upper wing is ahead of the lower wing, and decalage is positive when the upper wing is at a higher angle of incidence than the lower wing. Figure 1 illustrates these geometric relationships.

Several researchers have investigated dual-wing systems,[1-4] however, Nenadovitch[5] was the first investigator to discover improved aerodynamics. Nenadovitch conducted two-dimensional tests with dual-wing configurations and with the equivalent single wing. His tests showed that a stagger of 1.0, a gap of 0.33, and a decalage of -6 deg achieved the greatest increase in performance over the equivalent single wing. All three of these optimum configuration parameters were at the extreme end of the range of values investigated.

In 1974, Olson and Selberg[6] compared dual wings and single wings of the same lift capacity in experiments with three-dimensional models. Their findings showed that dual-wing configurations could achieve substantially higher lift-to-drag ratios than a single wing at lift coefficients below $C_{l_{max}}$. In 1979, Wolkovitch[7] investigated tandem wing configurations for VSTOL applications. All of his configurations had negative stagger and the experimental results illustrated the lower induced drag predicted by the Munk-Prandtl-Tietjens theory.[8-10] His results also indicated that at the higher lift coefficients the span efficiency of the dual-wing configuration was higher than the single-wing configuration. Addoms and Spaid[11] did an aerodynamic analysis of high-performance dual wings where they tailored the wing's

Received Dec. 10, 1982; revision received June 28, 1983. Copyright © American Institute of Aeronautics and Astronautics, Inc., 1983. All rights reserved.

*Former Graduate Student, Mechanical and Aerospace Engineering Department.

†Professor of Aerospace Engineering, Mechanical and Aerospace Engineering Department. Member AIAA.

camber to compliment the induced flowfield of the dual wings in order to maintain the same $C_{l_{max}}$ as the single-wing configuration. Their final dual-wing design configuration gave superior low-speed maneuverability, short field performance, load carrying capability, and lower cost than their single-wing aircraft comparison.

Several authors have recently modified the original analysis of Munk-Prandtl-Tietjens[8-10] for canard wing or tandem wing configurations. Laitone[12] modified Prandtl's induced drag equation to account for nonelliptical span lift distributions. However, he presented results for only constant and elliptically loaded cases. Kroo[13] has solved for the minimum induced drag of canard configurations by extending Prandtl's analysis. His results assume the canard is elliptically loaded and his results add one additional correction to the classical result. Butler[14] analyzed canard wing configurations of infinite span for the purpose of calculating induced drag. His results showed an induced thrust that increased as gap decreased and was a maximum for canard span to wing span ratios of one-half. With the exception of Butler's work all of the induced drag results are for relatively large gap-to-span ratios, whereas Butler's is for infinite stagger.

Several investigators have analytically studied dual-airfoil effects. Most of the early work investigated slat-airfoil effects of airfoil-flap effects. In 1972, Liebeck[15] investigated the aerodynamics of slat-airfoil combinations. This study was attempting to maximize the lift coefficient through the use of slats. No drag data was presented, moreover, no discussion or maximizing took place at cruise-type conditions. Lissaman and O'Pray[16] developed a semi-inverse technique to design optimum slats for a given airfoil. They did not discuss drag morslat orientation with respect to reported results. In 1974, Smith,[17] in the Wright Brothers Lecture, gave an extensive discussion of high-lift aerodynamics. He discussed slats, flaps, and multielements all with respect to high lift. He proved that a two-element airfoil can produce more lift than a single-element airfoil. However, he did not consider the drag benefits or penalties of multielement airfoil systems. Moreover, he did not consider typical cruise conditions and the lift-to-drag ratio at these conditions.

In 1980, Rokhsaz,[18] also using analytical methods, determined that dual-airfoil systems could reduce two-dimensional drag by 13-20% over an equivalent single-airfoil system. In addition, he discussed the mechanisms which caused this phenomenon.

The current study is intended first to find the dual-wing and SFSR wing which attains the greatest performance improvements over a single wing, using two state-of-the-art airfoil sections, the MS(1)-0313[19] and the laminar NL(S)-0715F,[20] which has recently been given the official NASA designation of NLF-0215F. The second phase of this study involves the design and performance comparison of several single-wing "baseline" aircraft and of corresponding dual-wing and SFSR-wing aircraft to determine the advantages and disadvantages of these dual-wing aircraft designs. All dual-wing studies will consider only dual wings of equal chord length.

Dual-Airfoil, Two-Dimensional Tradeoff Studies

A detailed parametric study was conducted to analytically determine the combination of stagger, gap, and decalage which resulted in the greatest improvement in the wing lift-to-drag ratio, L/D, in terms of both two-dimensional viscous drag and three-dimensional induced drag results. For small staggers the results of Rokhsaz[18] indicated that the most favorable configuration, on the basis of two-dimensional performance only, was a stagger of 1.0, a gap of 0.26, and a decalage of -6 deg for the NACA 63_2-215 airfoil. Using this placement of the airfoil system as the starting point for the two airfoils considered in this study [the MS(1)-0313 and the NL(S)-0715F], the parametric investigation was performed by holding the initial values of two of these parameters constant while changing the value of the third variable.

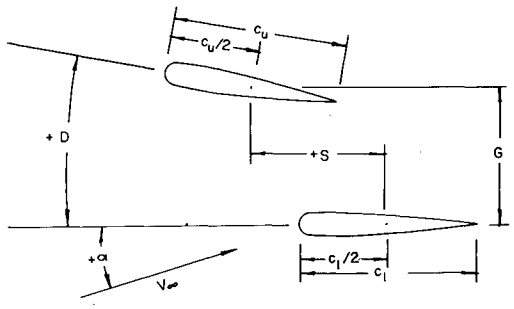

NOTE: S and G are nondimensionalized with respect to c_l

Fig. 1 Dual-airfoil geometric relationships.

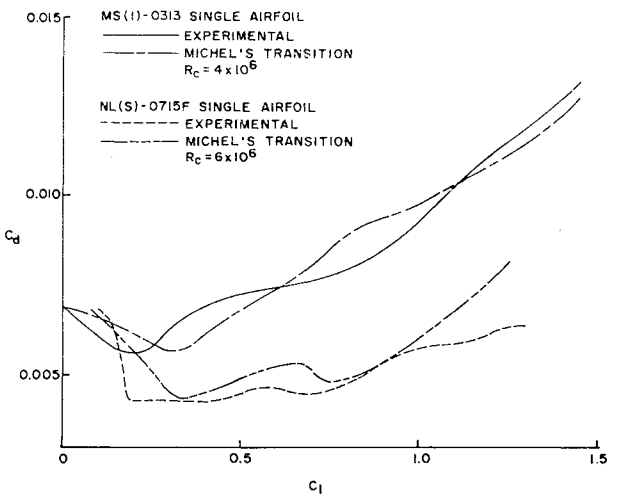

Fig. 2 Comparison of theoretical with experimental results.

The parametric study utilized an inviscid vortex panel multielement airfoil program[18] where the airfoils are represented by polygon approximations. Typical cases involved using 48 panels per airfoil. The inviscid multielement program was joined to a momentum integral boundary-layer analysis program to compute theoretical two-dimensional viscid and inviscid data. The laminar flow portion of the momentum integral program predicts the behavior of the boundary layer with Thwaites' method[21] and uses Michel's transition criterion[22] to determine the point of laminar-turbulent transition. The turbulent flow solution is then obtained by Head's momentum integral method[23] and the viscous drag is calculated with the Squire-Young formula.[24] This program set allows computation of complete multielement aerodynamic coupling, including thickness effects which become important at small gaps. Viscous drag predictions from the combined vortex panel viscous boundary-layer program were compared to experimental results[19,20] at the same Reynolds numbers to determine the degree of correlation between experimental and analytical results. Figure 2 compares the theoretical and experimental data for the MS(1)-0313 airfoil at a Reynolds number R_c of 4×10^6 and for the NL(S)-0715F at a Reynolds number of 6×10^6. This good agreement was achieved by using a Young's factor of 2.4 for the MS(1)-0313 and 2.2 for the NL(S)-0715F in the Squire-Young equation. Similarly good results were obtained at other Reynolds numbers for both airfoils.

Initial investigation of the performance of various dual-wing configurations covered a wide range of staggers to confirm the observations of previous dual-wing research.[5,6,18] Figures 3 and 4 present the findings of this investigation and a comparison with the single-wing data for the MS(1)-0313 airfoil. In Fig. 3, the negative-stagger runs (curves E through H) invariably exhibited flow separation at relatively low lift

Downloaded by ISAE on October 25, 2021 | http://arc.aiaa.org | DOI: 10.2514/3.48234

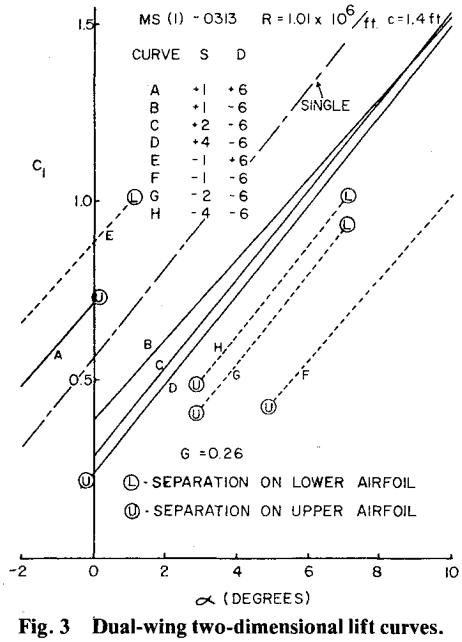

Fig. 3 Dual-wing two-dimensional lift curves.

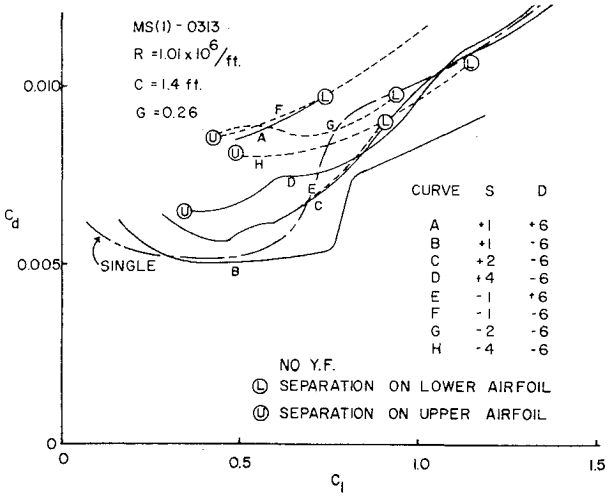

Fig. 4 Dual-wing two-dimensional drag polars.

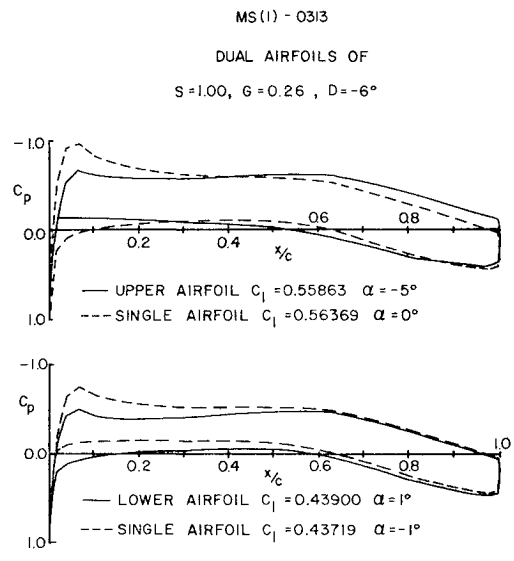

Fig. 5 Single- and dual-wing pressure distributions.

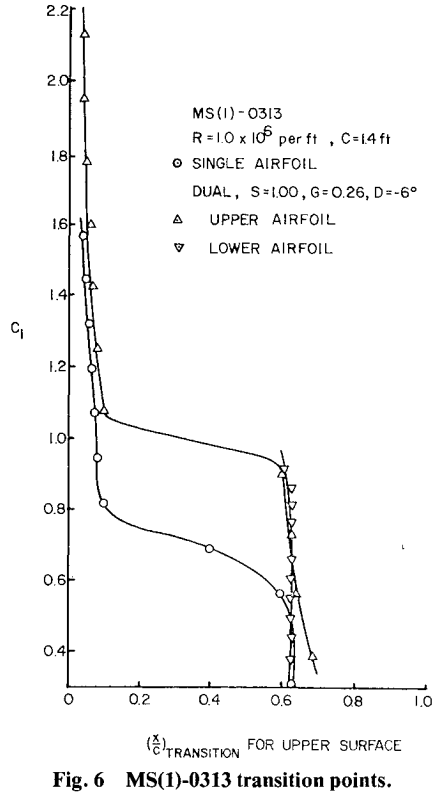

Fig. 6 MS(1)-0313 transition points.

coefficients, while the positive-stagger, negative-decalage cases (curves B through D) delayed the separation point to lift coefficients of 1.5 or greater. The positive-stagger, positive-decalage run (curve A) separated at a lift coefficient of less than 0.8, and produced an excessive amount of drag, as shown in Fig. 4. Likewise, the negative-stagger configurations created large amounts of drag in relation to the positive-stagger, negative-decalage cases. All of these findings supported the conclusions reached by Norton,[1] Nenadovitch,[5] and Olson and Selberg,[6] who determined that both the negative-stagger and the positive-decalage configurations performed poorly compared with the positive-stagger, negative-decalage condition. The NL(S)-0715F airfoil displayed similar behavior.

With the negative-stagger and positive-decalage cases rejected for their poor performance, the stagger, gap, and decalage angle changes were varied to find the optimum positive-stagger configuration.

Figure 5 shows the pressure distribution for two airfoil sections that are closely coupled; a stagger of 1.0, a gap of 0.26, and a decalage of -6 deg. For this case, the lower wing at a geometric angle of attack α of 1 deg obtained a lift coefficient C_l of 0.439, comparable to that of a single wing at a -1 deg angle of attack. The upper wing produced a lift coefficient of 0.559 at a geometric angle of attack of -5 deg, which is approximately equal to the lift on a single wing at a 0 deg angle of attack. Thus, the upper and lower wings receive a $+5$ and -2 deg induced angle of attack, respectively, indicating that the flow about each wing is significantly affected by the presence of the other wing. Figure 5 also illustrates the reduced leading-edge pressure peak and the reduced adverse pressure gradient experienced by the dual wings, both of which inhibit boundary-layer separation. Smith[17] refers to the dual-airfoil aerodynamic coupling in terms of five effects: slat effect, circulation effect, dumping effect, off-the-surface pressure recovery, and fresh boundary-layer effect. The "slat" effect reduces the pressure peak at the leading edge. The downstream airfoil causes the trailing edge of the upstream airfoil to be in a region of high velocity, thereby increasing the "circulation" on the forward airfoil. Since the

Downloaded by ISAE on October 25, 2021 | http://arc.aiaa.org | DOI: 10.2514/3.48234

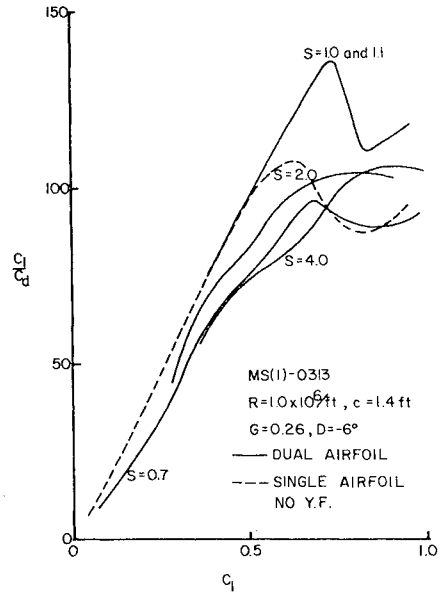

Fig. 7 MS(1)-0313 two-dimensional stagger study results.

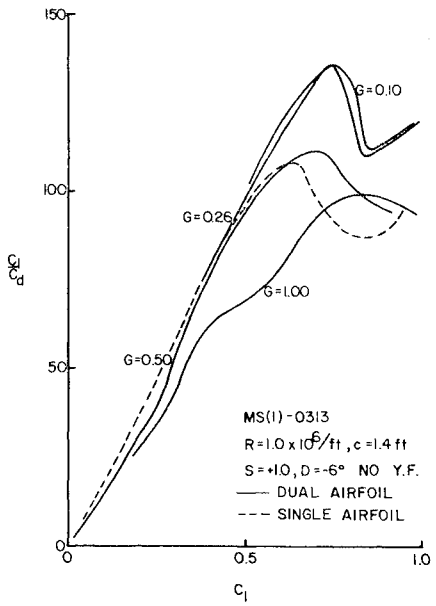

Fig. 8 MS(1)-0313 two-dimensional gap study results.

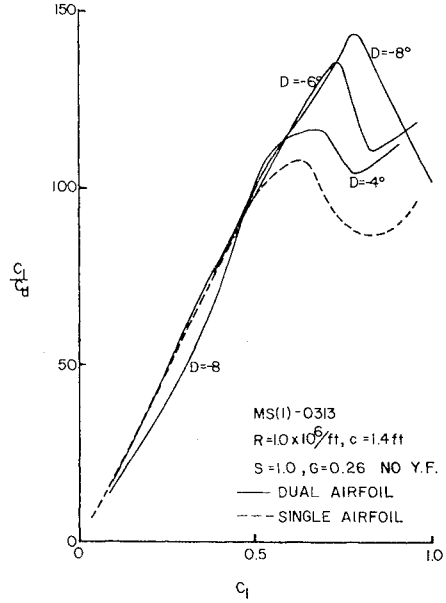

Fig. 9 MS(1)-0313 two-dimensional decalage study results.

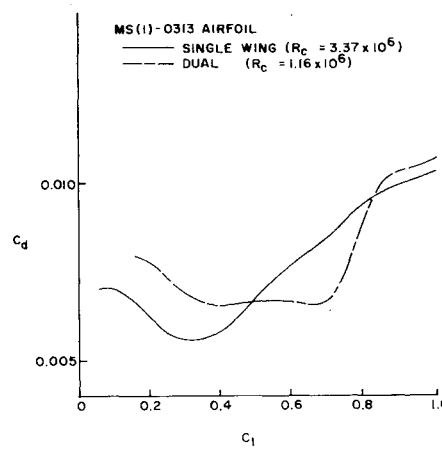

Fig. 10 Two-dimensional drag comparison.

trailing edge of the forward airfoil is in a region of high velocities the boundary layer "dumps" at a very high velocity. The boundary layer is dumped at velocities higher than freestream allowing the "off-surface pressure recovery." Finally each new airfoil starts with a "fresh new boundary layer."

Upper surface transition location for a stagger of 1.0, a gap of 0.26, and a decalage of −6 deg is shown in Fig. 6. The transition points for both the dual- and single-wing configurations were at about 60% and 10% chord for low- and high-lift coefficients, respectively. However, the shift from transition at 60% chord to transition at 10% chord occurred at lift coefficients of 0.6-0.8 for the single wing, as opposed to 0.9 to 1.1 for the dual-wing configuration. The essence of this behavior is that the dual wing benefits from a considerably longer period of laminar flow between lift coefficients of 0.6 and 1.1 and a corresponding decrease in viscous drag.

Results of the parametric study for the MS(1)-0313 airfoil are shown in Figs. 7-9. These figures illustrate relative comparisons at the same Reynolds number and do not contain the Young's factor correction. Figure 7 depicts the two-dimensional results of the constant-gap, constant-decalage, variable-stagger runs and, for comparison, the single-wing performance. A significant increase over the single-wing C_l/C_d curve was obtained with staggers of 1.0 and 1.1. Performance fell off as stagger was increased or decreased from this optimum stagger range.

The two-dimensional, variable-gap analysis is summarized in Fig. 8. With stagger and decalage held at 1.0 and −6 deg, respectively, the highest performance was obtained at gaps of 0.10 and 0.26. Lift-to-drag ratios dropped considerably as gap increased beyond 0.26. The 0.1 gap case was not used to avoid any flow blockage which might occur.

Figure 9 presents the data for the variable-decalage, two-dimensional runs. Overall, the best small stagger performance was obtained with a −6 deg decalage. An −8 deg decalage produced a higher maximum lift-to-drag ratio than did the −6 deg decalage case, but the latter held the performance edge at lift coefficients of 0.5 and below.

A typical dual-wing configuration would have a lower chord Reynolds number than the single wing. Figure 10 shows the two-dimensional drag of the dual and single airfoils. $S=1.0$, $G=0.26$, and $D=-6$ deg for the dual airfoils. The Reynolds number of the dual is 1.16×10^6, whereas the single is double the dual, or 3.37×10^6. The drag bucket has been

Downloaded by ISAE on October 25, 2021 | http://arc.aiaa.org | DOI: 10.2514/3.48234

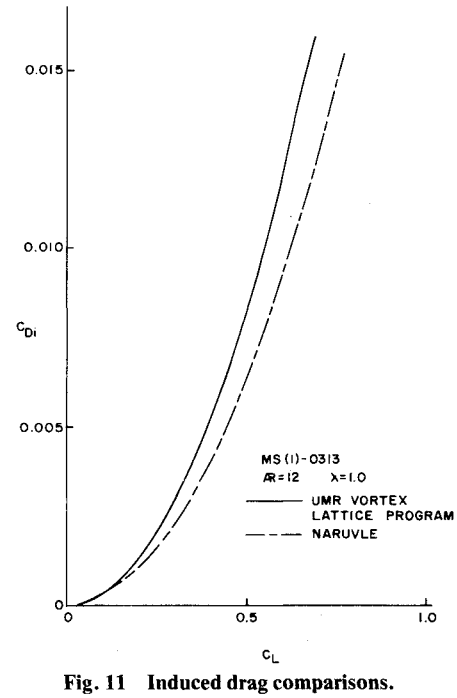

Fig. 11 Induced drag comparisons.

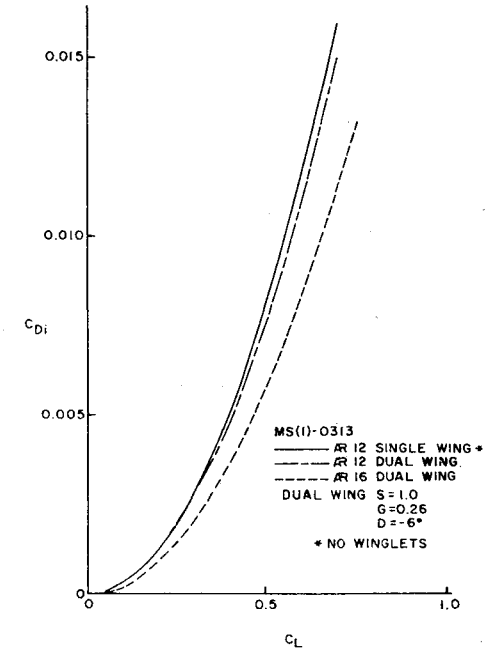

Fig. 13 Typical induced drag curves for the MS(1)-0313 airfoil.

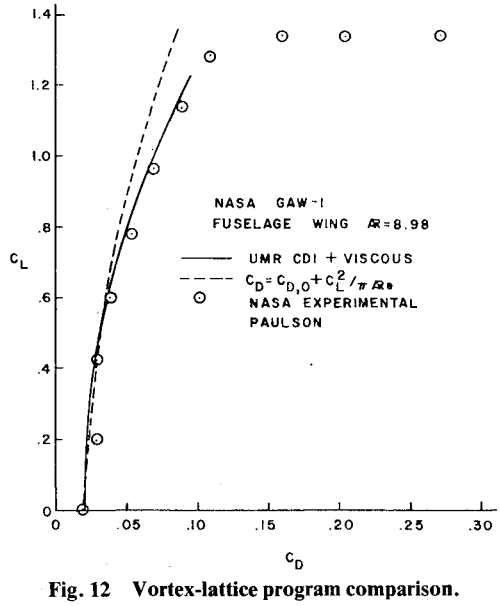

Fig. 12 Vortex-lattice program comparison.

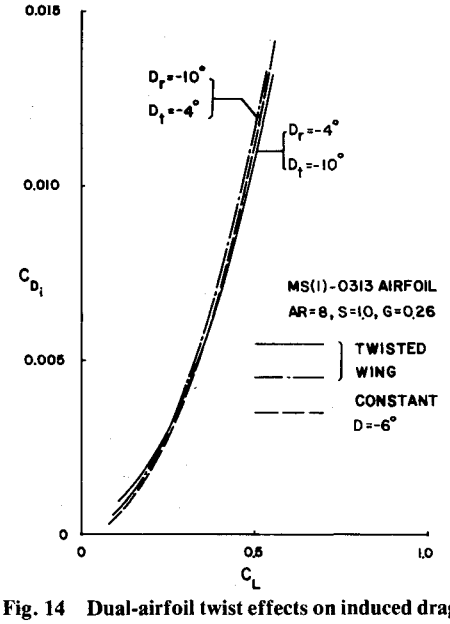

Fig. 14 Dual-airfoil twist effects on induced drag.

shifted to the right giving the dual airfoil lower drag at the higher lift coefficients.

This optimal dual-airfoil placement, $S=1.0$, $G=0.26$, and $D=-6$ deg was used for the SFSR configuration at the tip with the remainder of the wing geometry being varied to give the lowest total drag. Due to the sweep of the wings on the SFSR configurations it was necessary to determine if spanwise contamination was significant, hence negating the two-dimensional boundary-layer results. Calculation of Re based on momentum thickness which were made after Beasley[25] verified that spanwise contamination was not important for conditions under consideration.

Dual-Airfoil, Three-Dimensional Tradeoff Studies

The two-dimensional results indicated that the maximum l/d improvement for the dual airfoils occurred at a small gap, $G=0.26$. At this gap there is strong aerodynamic coupling and the differences in C_{l_0} predictions using vortex panel results which include thickness vs vortex-lattice results which ignore thickness is about 60%.[26] Since all the methods discussed earlier[8-10,12-14] did not account for thickness, and since the gaps are such that thickness is important, a vortex-lattice method, which utilized C_{l_α} and C_{l_0} data from the vortex panel program,[22] was used to predict induced drag. Figure 11 shows the results of this program compared to NARUVLE[28] a vortex-lattice program without a thickness correction. The University of Missouri-Rolla (UMR) vortex-lattice program predicts higher values of induced drag than NARUVLE. A comparison of the UMR vortex-lattice program with a wing fuselage NASA model $AR=8.9$ after Paulson[29] is shown in Fig. 12. There is excellent agreement up to the beginning of boundary-layer separation.

Aspect ratio, taper, stagger, gap, decalage, and twist studies were conducted for the closely coupled dual wing configurations and the SFSR configuration. Figure 13 shows the effect of aspect ratio for the closely coupled dual wing as compared to the single wing illustrating the slight induced

Downloaded by ISAE on October 25, 2021 | http://arc.aiaa.org | DOI: 10.2514/3.48234

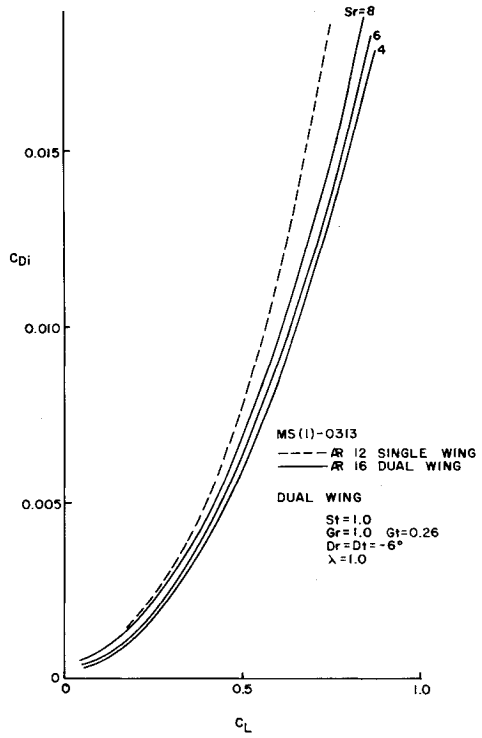

Fig. 15 Effects of stagger on induced drag for SFSR configuration.

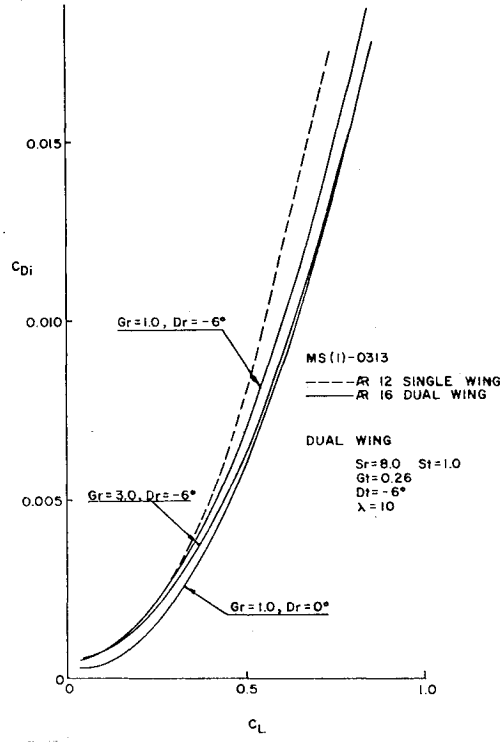

Fig. 16 Gap and decalage effects on induced drag for SFSR configuration.

drag advantage of the dual wing over a single wing of equivalent aspect ratio, i.e., a single airfoil with the same span, b, and area, S_{ref}, as the dual wing, and whose chord is equal to the sum of the two dual wing chords. The figure also indicates the significantly lower induced drag of the aspect ratio 16 wing compared to the wing of aspect ratio 12. Taper ratio studies were conducted for closely coupled dual wings, S=1, G=0.26, and D=−6 degrees. The results indicated minimum drag was obtained for taper ratios of 0.4 and 0.6. A taper ratio of 0.6 was used because it allowed a larger chord. Twist studies were also conducted. An example of these results is shown in Fig. 14 for the MS(1)-0313 airfoil. There is a slight reduction in induced drag for geometric washout and a slight increase for geometric washin. On the basis of the two-dimensional viscous drag and the three-dimensional induced drag results, the optimum closely coupled dual-wing configuration was determined to be a stagger of 1.0 and a gap of −6 deg with a taper ratio of 0.6.

Induced drag studies were also conducted for the SFSR configuration. Figure 15 shows the effect of stagger on induced drag for the SFSR configuration with the lowest stagger configurations having the least induced drag. Figure 16 shows the effects of gap and decalage variation with span for a fixed stagger at the wing root. The geometry at the tip was chosen to be that which gave the optimum improvements in the closely coupled two-dimensional study. As the figure illustrates, the best configuration has a gap of 1.0 at the wing root and a decalage of zero at the root.

The two-dimensional parametric study was also conducted with the NL(S)-0715F airfoil section. The same transition and lift-over-drag trends were found to occur except at much higher lift coefficients. The NL(S)-0715F dual-airfoil transition delay did not occur until lift coefficients greater than 1.0 were realized. This is because below lift coefficients of 1.0 most of the surface has laminar flow, hence, the coupling can not produce a significantly greater laminar run. Above lift coefficients of 1.0 most of the surface has laminar flow, hence, the coupling can not produce a significantly greater laminar run. Above lift coefficients of 1.0 the dual-airfoil improvements were again realized, although not to as great an extent. From the two-dimensional results for the NL(S)-0715F airfoil section the optimum configuration for the wing was a stagger of 1.0, a gap of 0.26, and a decalage angle of −6 deg. All induced drag trends followed those of the MS(1)-0313 airfoil section.

Design of the Baseline and Dual-Wing Configurations

The performance figures produced by this parametric study were used to design 12 aircraft: a six-place and a twelve-place "baseline" aircraft, a six-place and a twelve-place closely coupled dual-wing aircraft, and a six-place and a twelve-place SFSR aircraft. Each of these six configurations were evaluated with the MS(1)-0313 and the NL(S)-0715F airfoil sections, making a total of 12 designs. The two baseline aircraft were of conventional single-wing, aft-tail configuration and were used as reference points. The dual-wing aircraft and SFSR wing aircraft, which used the same fuselage, tail, and power plant as the corresponding baseline aircraft, were compared to these reference points to ascertain the merits of these dual-aircraft designs.

The 12 aircraft in this study were designed for a 563 km/h (350 mph) cruise speed at altitudes of 9,144-12,192 m (30,000-40,000 ft) and a range of 2414 km (1500 miles) or more. The baseline aircraft were limited to aspect ratios of 6-12 and wing loadings of 1197-2873 N/m^2 (25-60 psf). However, due to the structural advantages gained by connecting the two wings at their wing tips, the dual-wing designs were limited to aspect ratios of 16 or less, rather than 12, as was the case with the baseline aircraft. Aspect ratio was defined as the square of the wing span divided by the total projected area of the two wings. For each wing configuration, two separate aircraft designs were required, both a six- and twelve-place airplane. The six-place aircraft was designed for 5338 N (1200 lb) payload and was intended as a personal or small business airplane, while the twelve-place aircraft, with twice the payload of the six-place, was meant to compete in the business aircraft market. All of the aircraft in this study were designed with lifting surfaces made of composite materials.

The fuselage was sized first. The height and width of the six- and twelve-place fuselages were sized to present minimum frontal area, and thus create minimum drag, while providing

Downloaded by ISAE on October 25, 2021 | http://arc.aiaa.org | DOI: 10.2514/3.48234

Downloaded by ISAE on October 25, 2021 | http://arc.aiaa.org | DOI: 10.2514/3.48234

interior volume for pilot, passengers, and luggage. The width of the twelve-place fuselage also was influenced by the requirement for a 30.5 cm (12 in.) aisle between the seats. The seat pitch, or the distance between adjacent rows of seats, was set at 91.4 cm (36 in.) for both versions. The passenger and luggage compartments for each version were then enclosed in a pressure vessel designed to provide a cabin pressure altitude of 2,438 m (8,000 ft) at an actual altitude of 12,192 m (40,000 ft). The rest of each fuselage was sized to provide space for the landing gear, power plant, avionics, and environmental control unit. No space was required for the fuel, since the fuel tanks were placed in the wings.

The six-place fuselage was built around a 132-cm (52-in.) high, 112-cm (44-in.) wide, 4.42-m (14.5-ft) long pressure cabin containing the six seats (in three rows of two seats each) and a luggage area aft of the last row of seats. The fuselage was designed for a conventional tricycle landing gear arrangement, with the nose gear housed below and forward of the pressure cabin and with the main gear located below and aft of the luggage compartment. The main gear retract aft into the fuselage. The gear arrangement exceeds the FAR overturning criteria. The single-turboprop engine was buried in the aftmost section of the fuselage tail cone. Air inlets for the engine were situated on either side of the fuselage and the propeller shaft was extended through the aft fuselage. The avionics and the environmental control unit were also housed in the fuselage aft of the pressure cabin.

The twelve-seat fuselage consisted of six rows of two seats and a baggage compartment aft of the last seat row. A 30.5 cm (12 in.) center aisle was also provided. The passenger and cargo areas were enclosed by a 163-cm (64-in.) high, 163-cm (64-in.) wide, and 7.37-m (24.2-ft) long pressure vessel. The tricycle gear were placed in approximately the same relative positions with respect to percentage of fuselage as were the landing gear for the six-place fuselage. The two turbofan engines were mounted on horizontal pylons attached to the aft fuselage. The avionics and environmental control units were placed in the aft fuselage. The dual-wing designs used the same fuselage as the baseline except for minor modifications, such as the addition of a fuselage fuel tank and minor rearrangement of internal systems. The wing fuel tanks of the dual wing were able to hold only about 50% of the required fuel.

The six-place aircraft used a scaled version of the Pratt and Whitney PT6-A45A turboprop engine[30] with a 2.29-m (90-in.)-diam four-bladed propeller. Specified fuel consumption was assumed to be a constant 0.344 kg/kW-h (0.55 lb/hp-h). The twelve-place aircraft used twin turbofan engines scaled from engines from a General Aviation Turbine Engine (GATE) study.[31] A 0.061 kg/N-h (0.6 lb/lb-h) thrust specific fuel consumption was assumed. The turboprop engine weight was scaled by the ratio of required power to production power, while the turbofan engine weight was scaled by the ratio of required thrust to reference engine thrust.

All aircraft were designed to utilize winglets to reduce the induced drag. A computer winglet study was conducted on a wing of aspect ratio 12 with taper ratios of 0.2-1.0, using the NARUVLE vortex-lattice program to compute the induced drag of the various configurations. Using a NASA winglet study[32] as a guide, the dihedral and incidence of the winglets were varied to find the configuration that provided the greatest reduction in induced drag. The optimum configuration agreed with Ref. 32 in terms of dihedral and incidence, although the magnitude of the predicted drag reduction was less. Because of the high degree of correlation between the current study and the NASA study, it was decided to use the standard NASA winglet design of Ref. 32. To be conservative, the drag reduction value obtained from NARUVLE was used, rather than that of Ref. 32. A taper ratio of 0.8 was chosen for the baseline.

For both dual-wing aircraft, because of the absence of information on the effectiveness of winglets on dual wings, it was conservatively assumed that the addition of winglets on dual wings would reduce the induced drag by approximately half the percentage of drag reduction achieved by winglets on a single wing. A taper ratio of 0.6 was found to create the least induced drag for the closely coupled dual-wing configuration, while a taper ratio of 1.0 gave the least induced drag for the SFSR configuration.

For the SFSR configuration all longitudinal control forces must be exerted by the wings, which implies a large stagger. Thus, the minimum root stagger which provided a $C_{m\delta_E}$ equal to the baseline was chosen. This occurred at $S_{\text{root}} = 8$. A gap of 3 was chosen to put the wings at the top and bottom of the fuselage.

Aircraft weight estimates were obtained with the aid of equations from Nicolai[33] and Torenbeek[34,35] and from a UMR design project,[36] a four-place, high-speed general aviation aircraft that utilized NASTRAN prediction methods.

Using equations from Nicolai with the UMR four-place design as a reference aircraft, the fuselage and empennage weights were determined for the six- and twelve-place aircraft under consideration. Nicolai's equations were used as scaling factors on the above reference weights. Wing weights were obtained for the six-place MS(1)-0313 configurations from NASTRAN-SEMOBEAM[37] computer optimization results. Wing weights for the six-place NL(S)-0715F configurations and all twelve-place configurations were obtained from a modification of Torenbeek's formula to account for the composite wings, and, for the dual-wing aircraft, Torenbeek's formula was calibrated using the six-place MS(1)-0313 configuration results. It was decided to structurally connect the dual wings only at the tip and the first bending moment location to minimize the added drag due to these structural connections. The NASTRAN-SEMOBEAM results demonstrated that the connection at the first bending moment location was not needed. With the structural connection only at the wing tip in the form of a structural winglet any additional drag would occur only at this location. This possible additional drag was accounted for by reducing the induced drag due to the structural winglets by one-half the winglet induced drag savings on the single wing. While lighter dual wings could have been designed using more structural connections, the uncertainty in the added strut drag would have overshadowed the structural savings. An ultimate load factor of 5.7, calculated from a 3.8 g load with a safety factor of 1.5, was used. Engine weight was obtained by scaling up the reference aircraft engine weight, using as a scaling the ratio of required thrust to the references aircraft required thrust. Miscellaneous weights were obtained with Nicolai's equations.

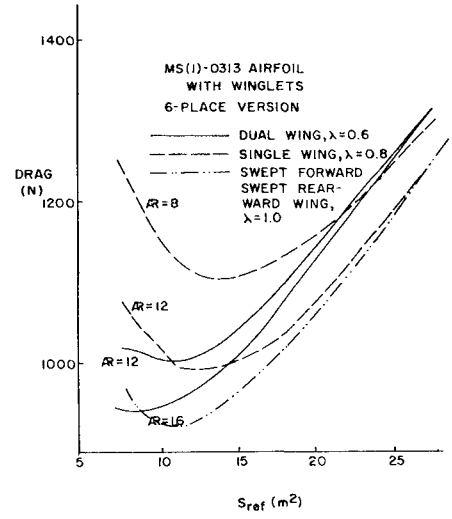

Fig. 17 Six-place aircraft, sample optimization curves.

Downloaded by ISAE on October 25, 2021 | http://arc.aiaa.org | DOI: 10.2514/3.48234

Estimates of total aircraft drag coefficient were obtained by the component buildup method. The drag coefficients of each component, weighted by the ratio of the component area to the aircraft reference area, were totaled and multiplied by 1.1 to account for interference effects, as suggested in Ref.35.

The drag of the lifting surfaces, the wing and horizontal tail, was predicted with the programs described above. For each cruise lift coefficients being investigated, the viscous drag at the proper Reynolds number and the induced drag at the desired aspect ratio, taper ratio, and sweep angle were added to get a total wing drag coefficient. A factor of 0.0005, or 5-10% of the zero-lift drag coefficient for the airfoils under consideration, was added to this wing drag coefficient to account for interference.

Graphs and equations for turbulent flow about streamlined bodies from Roskam,[38] Hoerner,[39] and Crawford[40] were used to estimate the drag contributions of essentially nonlifting components. These drag coefficients, separately weighted by the ratio of component reference area to the aircraft reference area, were then added to get the total drag coefficient due to nonlifting components. To account for interference drag, this drag coefficient was increased by 10%.

The wing area was then optimized. A computer code would scan through a range of wing areas to find the area which created the least cruise drag. For each wing area in the desired range, the program computed the total aircraft cruise weight W_{cr} assuming constant engine weight, which determined the cruise lift coefficient. The program then searched through the two- and three-dimensional drag polars to find the viscous and induced drag coefficients of the wing at the desired lift coefficient for the specified conditions; namely, cruise Reynolds number and aspect ratio. Engine weight was then recalculated based on required cruise power before the final drag minimization which was the criteria by which the program selected the optimum wing area. All aircraft were optimized for cruise performance only with no attempt to take into account takeoff, climb, or landing performance. However, all aircraft were designed and checked to assure takeoff rotation.

Figure 17 shows a sample of the results of the optimization program for the six-place aircraft with wings of MS(1)-0313 section and aspect ratios of 8 and 12 for the single wing and aspect ratios of 12 and 16 for the dual and SFSR configurations. Over a wing area range of 7-28 m^2 (75-301 ft^2), the minimum cruise drag for the single-wing aircraft was obtained at an area of 12.9 m^2 (140.0 ft^2) for the case of $AR = 12$. For the closely coupled dual-wing aircraft the minimum drag was obtained at an area of 7.7 m^2 (84.0 ft^2) for the case of $AR = 16$. The SFSR wing aircraft obtained a minimum drag at an area of 10.5 m^2 (114.8 ft^2) for the case of $AR = 16$.

On the basis of the results of the optimization program, a cruise altitude of 12,192 m (40,000 ft) was selected to be the best cruise altitude. Since the study was limited to aspect ratios of 12 or less for the single wing, the $AR = 12$ case was chosen. For the closely coupled dual wing and the SFSR wing with their enhanced wing structural capability due to the wing connections an aspect ratio of 16 was selected.

After the optimum wing areas were determined, a final sizing of the horizontal and vertical tails was required to provide longitudinal, lateral, and directional stability. With the center of gravity placed at its most unfavorable position, the horizontal and vertical tail areas were varied until each aircraft was statically stable. The degree of static stability attained was comparable to that found in typical light and business aircraft. The static stability analysis was performed using the techniques of Roskam.[41,42]

Once the horizontal tail size was known, the trimmed performance of each aircraft was estimated. The required tail lift coefficient for zero pitching moment in cruise was computed, and this tail lift coefficient was used to find the tail drag coefficient at the trimmed condition, using the momentum integral boundary-layer and vortex-lattice programs described previously. This additional trim drag was calculated and the untrimmed data obtained from the optimization program was modified accordingly. Drag penalties due to train were less than 3% of the total drag.

Table 1 gives the final results for the six-place, single- and dual-wing aircraft. For both airfoil sections, Table 1 gives the cruise weight, wing weight, engine weight, drag, power, and lift coefficients at trimmed cruise conditions. Also shown is the lift-to-drag ratio in cruise wing area and range for each aircraft.

The lift-to-drag ratios achieved by these baseline aircraft were markedly higher than most contemporary light and business aircraft. Holmes and Croom[30] indicate that current technology six-place aircraft have maximum lift-to-drag ratios of about 14 at 556 km/h (300 knots) cruise speeds. The baseline six-place aircraft in the current study attained cruise lift-to-drag ratios of more than 19 at 563 km/h (350 mph), or 36% improvement. This greatly improved performance can be attributed to the superior airfoil sections used on the baseline aircraft as well as to the higher aspect ratios found on the aircraft of this study. The dual-wing and SFSR six-place aircraft both attained cruise lift-to-drag ratios of more than 20 at 563 km/h, which is a 48% improvement. The addition of winglets to these aircraft also contributed to their superior performance.

Figure 18 shows the exterior projected view of the finished six-place baseline, dual-wing, and SFSR aircraft.

Table 2 gives the final modified trimmed results of the single-, dual-, and SFSR design process for the twelve-place aircraft. Again, the dual-wing and SFSR wing configurations outperform the single wing for both airfoil sections.

For both the six- and twelve-place aircraft the dual-wing configurations with their higher L/D ratios are operating

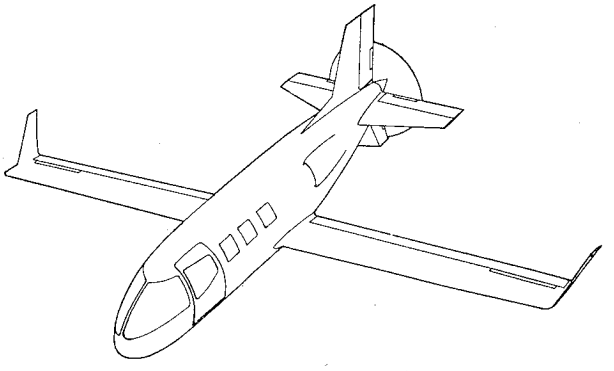

Fig. 18a Baseline-exterior view.

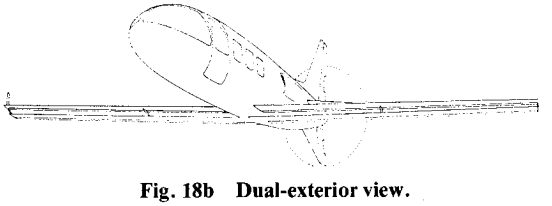

Fig. 18b Dual-exterior view.

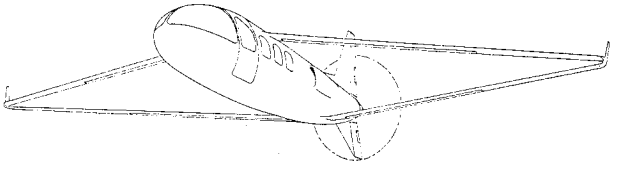

Fig. 18c Swept forward/swept rearward-exterior view.

Downloaded by ISAE on October 25, 2021 | http://arc.aiaa.org | DOI: 10.2514/3.48234

Table 1 Design performance—Minimum Cruise Drag (trimmed six-place with winglets)

	W_{cr}, N (lb)	W_{eng}, N (lb)	W_{wing}, N(lb)	$C_{L_{cr}}$	D_{cr}, N (lb)	P_{req}, kw (hp)	$\frac{\Delta P_{req}}{P_{req}}$, %	$\left(\frac{L}{D}\right)_{cr}$	S_{ref}, m^2 (ft^2)	$\left(\frac{W}{S}\right)_{wing}$, N/m^2(lbf/ft^2)	R, km (miles)	$\frac{\Delta R}{R}$, %
						MS(1)-0313						
Single-wing[a]	19,673	3,483	1,806		1,018	159			12.9	1,534	2,757	
baseline	4,423	(783)	(406)	0.41	(229)	(213)		19.28	(140.0)	(31.6)	(1,713)	
Dual wing[a]	18,241	3,260	1,419		943	148			7.7	2,461	2,981	
	(4,271)	(733)	(319)	0.66	(212)	(198)	−7.3	20.13	(84.0)	(50.8)	(1,852)	8.1
SFSR[a]	18,827	3,154	1,503		908	142			10.5	1,831	3,095	
	(4,339)	(709)	(338)	0.49	(204)	(190)	−10.8	21.23	(114.8)	(37.8)	(1,923)	12.3
NL(S)-0715F												
Single-wing[b]	19,091	3,363	1,383		974	152			11.2	1,710	2,899	
Baseline	(4,292)	(756)	(311)	0.42	(219)	(204)	−4.2	19.66	(121.6)	(35.3)	(1,801)	5.4
Dual wing[b]	18,628	3,260	1,548		943	148			9.2	2,093	2,983	
	(4,316)	(733)	(348)	0.55	(212)	(198)	−7.0	20.39	(100.2)	(43.2)	(1,853)	8.2
SFSR[b]	17,140	3,047	1,245		872	136			7.9	2,355	3,231	
	(4,140)	(685)	(280)	0.63	(196)	(182)	−14.5	21.32	(86.0)	(48.6)	(2,007)	17.2

[a]NASTRAN weights. [b]Scaled NASTRAN weights.

Table 2 Design performance—Minimum Cruise Drag (trimmed twelve-place with winglets)

	W_{cr}, N (lb)	W_{eng}, N (lb)	W_{wing}, N(lb)	$C_{L_{cr}}$	D_{cr}, N (lb)	P_{req}, kw (hp)	$\frac{\Delta P_{req}}{P_{req}}$, %	$\left(\frac{L}{D}\right)_{cr}$	S_{ref}, m^2 (ft^2)	$\left(\frac{W}{S}\right)_{wing}$, N/m^2(lbf/ft^2)	R, km (miles)	$\frac{\Delta R}{R}$, %
						MS(1)-0313						
Single-wing[a]	33,809	3,856	2,953		1,797	281			19.7	1,720	2,971	
baseline	(7,601)	(867)	(664)	0.46	(404)	(376)		18.79	(214.0)	(35.5)	(1,846)	
Dual wing[a]	33,671	3,607	3,065		1,761	256			15.8	2,137	3,250	
	(7,570)	(811)	(689)	0.57	(369)	(343)	−8.8	20.45	(171.8)	(44.1)	(2,019)	9.4
SFSR[a]	32,941	3,572	2,904		1,601	250			19.0	1,735	3,467	
	(7,406)	(803)	(653)	0.48	(360)	(335)	−10.9	21.71	(207.0)	(35.8)	(2,154)	16.7
NL(S)-0715F												
Single-wing[b]	33,458	3,736	2,722		1,788	279			19.5	1,720	2,989	
Baseline	(7,522)	(840)	(612)	0.46	(402)	(374)	−0.5	18.71	(212.0)	(35.5)	(1,857)	0.5
Dual wing[b]	33,778	8,589	3,189		1,619	253			18.4	1,836	3,306	
	(7,594)	(807)	(717)	0.49	(364)	(339)	−9.8	20.83	(200.6)	(37.9)	(2,054)	11.3
SFSR[b]	32,453	3,483	2,504		1,503	235			14.5	2,233	3,565	
	(7,296)	(783)	(563)	0.60	(338)	(315)	−16.2	21.65	(158.2)	(46.1)	(2,215)	20.0

[a]NASTRAN weights. [b]Scaled NASTRAN weights.

Table 3 Design performance—constant wing loading (trimmed six-place with winglets)

	W_{cr}, N (lb)	W_{eng}, N (lb)	W_{wing}, N(lb)	$C_{L_{cr}}$	D_{cr}, N (lb)	P_{req}, kw (hp)	$\frac{\Delta P_{req}}{P_{req}}$, %	$\left(\frac{L}{D}\right)_{cr}$	S_{ref}, m^2 (ft^2)	$\left(\frac{W}{S}\right)_{wing}$, N/m^2(lbf/ft^2)	R, km (miles)	$\frac{\Delta R}{R}$, %
						MS(1)-0313						
Single-wing[a] baseline	19,949 (4,485)	3,683 (828)	1,623 (365)	0.54	1,081 (243)	169 (226)		18.81	10.1 (109.6)	1,982 (40.9)	2,654 (1,649)	
Dual wing[a]	19,513 (4,387)	3,309 (744)	1,552 (349)	0.54	956 (215)	149 (200)	−11.5	20.09	9.5 (103.7)	2,049 (42.3)	2,897 (1,800)	9.2
SFSR[a]	18,948 (4,260)	3,136 (705)	1,437 (323)	0.54	898 (202)	140 (188)	−16.8	20.81	9.3 (101.0)	2,044 (42.2)	3,092 (1,921)	16.5
NL(S)-0715F												
Single-wing[a] Baseline	19,665 (4,421)	3,416 (768)	1,592 (358)	0.54	992 (223)	154 (207)	−8.4	19.59	9.7 (105.2)	2,035 (42.0)	2,802 (1,741)	5.6
Dual wing[a]	19,487 (4,381)	3,269 (735)	1,561 (351)	0.54	943 (212)	147 (197)	−12.8	20.40	9.6 (104.0)	2,040 (42.1)	2,946 (1,830)	11.0
SFSR[a]	18,566 (4,174)	3,109 (699)	1,334 (300)	0.54	890 (200)	139 (186)	−17.7	21.02	9.3 (100.8)	2,006 (41.4)	3,187 (1,980)	20.0

[a] NASTRAN weights.

Table 4 Design performance—constant wing loading (trimmed twelve-place with winglets)

	W_{cr}, N (lb)	W_{eng}, N (lb)	W_{wing}, N(lb)	$C_{L_{cr}}$	D_{cr}, N (lb)	P_{req}, kw (hp)	$\frac{\Delta P_{req}}{P_{req}}$, %	$\left(\frac{L}{D}\right)_{cr}$	S_{ref}, m^2 (ft^2)	$\left(\frac{W}{S}\right)_{wing}$, N/m^2(lbf/ft^2)	R, km (miles)	$\frac{\Delta R}{R}$, %
						MS(1)-0313						
Single-wing[a] baseline	33,516 (7,535)	3,754 (844)	2,762 (621)	0.51	1,806 (406)	282 (378)		18.63	17.7 (192.2)	1,899 (39.2)	2,967 (1,843)	
Dual wing[a]	33,698 (7,576)	3,612 (812)	3,087 (694)	0.51	1,646 (370)	257 (344)	−9.0	20.46	17.4 (189.0)	1,943 (40.1)	3,282 (2,039)	10.6
SFSR[a]	32,826 (7,380)	3,527 (793)	2,833 (637)	0.51	1,552 (349)	243 (325)	−14.2	21.03	17.2 (186.8)	1,914 (39.5)	3,427 (2,129)	15.5
NL(S)-0715F												
Single-wing[a] Baseline	33,333 (7,494)	3,745 (842)	2,589 (582)	0.51	1,797 (404)	281 (376)	−0.5	18.58	17.5 (190.4)	1,909 (39.4)	2,988 (1,856)	0.7
Dual wing[a]	33,742 (7,586)	3,594 (808)	3,149 (708)	0.51	1,623 (365)	254 (340)	−10.0	20.82	17.8 (193.3)	1,899 (39.2)	3,297 (2,048)	11.1
SFSR[a]	32,666 (7,344)	3,501 (787)	2,700 (607)	0.51	1,521 (342)	237 (318)	−15.9	21.54	17.2 (187.3)	1,899 (39.2)	3,519 (2,186)	18.6

[a] Scaled NASTRAN weights.

Downloaded by ISAE on October 25, 2021 | http://arc.aiaa.org | DOI: 10.2514/3.48234

closer to their maximum L/D ratios. The wing loadings for these dual-wing aircraft under these conditions are also higher. This could cause stall speed problems relative to the single-wing aircraft. Although only cruise conditions were analyzed herein, Smith[17] has shown that two-element airfoils can achieve higher maximum lift coefficients than a single-element airfoil which will alleviate the problem.

The performance of these aircraft also can be compared at constant wing loading. Tables 3 and 4 present the performance results at constant wing loading. Wing loadings between the optimum single- and dual-wing cases were chosen for comparison.

Design Comparison and Recommendations

Comparing Tables 1 and 2, one notices the lower cruise drag of the dual- and SFSR-wing configurations. The drag of the closely coupled dual-wing cases was lower than that of the baseline aircraft by 7.3-8.8% for the MS(1)-0313 airfoil and 7-9.8% for the NL(S)-0715F airfoil. In terms of range, this means that for the same fuel, the closely coupled dual-wing aircraft achieved 9.4-12.3% more range than the baseline aircraft with the MS(1)-0313 airfoil and up to 8.2-11.3% more range with the NL(S)-0715F airfoil. The drag of the SFSR-wing configuration was 10.8-10.9% lower than that of the baseline aircraft for the MS(1)-0313 airfoil and 14.5-16.2% lower for the NL(S)-0715F airfoil. The range of the SFSR aircraft was 9.4-12.3% greater than the baseline for the MS(1)-0313 airfoil and 17.2-20.0% greater for the NL(S)-0715F airfoil.

The difference in optimum cruise lift coefficient is also outstanding. The optimum cruise lift coefficients for the baseline aircraft ranged between 0.41 and 0.46, while the dual- and SFSR-wing designs optimized at much higher lift coefficients, from 0.48 to 0.66, with correspondingly lower wing areas. Both dual-wing configurations are operating closer to their respective L/D maxima. The dual- and SFSR-wing aircraft also have lower engine weights than the baseline, which translates into lower engine acquisition costs. The wing weights of the dual-wing configurations that employed NASTRAN-SEMOBEAM weight predictions were also lower than their baseline configurations.

Comparing Tables 3 and 4, where essentially constant wing loading is maintained, the same basic trends occur for the dual and SFSR configurations; lower cruise drag and greater ranges. The actual magnitudes are also very close.

Some potential problems were noted with the dual-wing designs. The wing volume available for fuel was insufficient, requiring the fuel to be carried aft of the pressurized cabin. The possibility also exists that the dual-wing configuration have aeroelastic problems not experienced by the conventional single-wing configuration.

In outperforming the baseline aircraft, the dual designs had to overcome some disadvantages. The greatest disadvantage was the increase in drag coefficient as Reynolds number decreased. Since the wing chords of the dual aircraft were half that of the single-wing aircraft, the dual designs were penalized by higher drag coefficients due to the reduced Reynolds number. This disadvantage would be reduced or eliminated by using an airfoil section designed for very low Reynolds numbers, (from about 10^6 to 2×10^6). The two airfoil sections investigated in this study were designed for Reynolds numbers of $6\text{-}9\times10^6$, and suffer from a degradation of performance at lower Reynolds number.

A second disadvantage was the conservative structural approach taken in designing the dual wings. The utilization of more bracing could offer an optimized aerodynamic-structural configuration.

Third, to be conservative, the winglets on the dual-wing aircraft were given only half of the induced drag reduction achieved by the single-wing winglets. This last disadvantage may be removed by extensive research on winglet designs for the dual-wing configuration, as has been done for single-wing configurations in the past.

Also, no effort was made to reduce the fuselage weight of the dual-wing configurations due to the multiple attachment points and hence lower stress levels.

In spite of these conservative estimates used in the design process, the baseline aircraft designs offer a significant improvement in cruise performance as compared to current technology aircaft. The dual-wing designs, aside from all of their disadvantages, offer still higher cruise performance, and a corresponding decrease in fuel consumption. With further research into the multiwing aircraft system, such as static and dynamic structural testing, low Reynolds number airfoil design, specifically for dual-wing applications and dual-wing winglet research, the dual-wing aircraft should prove to be even more attractive.

Acknowledgments

The results presented in this paper were obtained from research funded by NASA Research Grant NAG1-26 administered by Langley Research Center under the direction of Dr. Bruce Holmes.

References

[1]Norton, F.H., "Effect of Staggering a Biplane," NACA TN-710, 1918.

[2]Knight, M. and Noyes, R.W., "Wing Tunnel Test on a Series of Biplane Wing Models, Part I. Effects of Changes in Stagger and Gap," NACA TN-310, 1929.

[3]Knight, M. and Noyes, R.W., "Wind Tunnel Tests on a Series of Biplane Wing Models, Part II. Effects of Changes in Decalage, Dihedral, Sweepback, and Overhand," NACA TN-325 1929.

[4]Knight, M. and Noyes, R.W., "Wind Tunnel Tests on a Series of Biplane Wing Models, Part III. Effects of Changes in Various Combinations of Stagger, Gap, and Decalage," NACA TN-330, 1929.

[5]Nenadovitch, M., "Recherches sur les Cellules Biplane Rigides d'Envergure Infine" Publications Scientifiques et Techniques du Minister de L'Air, Institut Aero'-technique de Saint-Cyr, Paris, 1936.

[6]Olson, E.C. and Selberg, B.P., "Experimental Determination of Improved Aerodynamic Characteristics Utilizing Biplane Wing Configurations," *Journal of Aircraft,* Vol. 13, April 1976, pp. 256-261.

[7]Wolkovitch, J., "Subsonic V/STOL Configurations with Tandem Wings," *Journal of Aircraft,* Vol. 16, Sept. 1979, pp. 605-611.

[8]Munk, M.M., "General Biplane Theory," NACA 151, 1921.

[9]Prandtl, L., "Induced Drag of Multiplanes," NACA TN-182, March 1924.

[10]Prandtl, L. and Tietjens, O.G., *Applied Hydro- and Aeromechanics,* Dover Publications, Inc., New York, 1957, pp. 213-216.

[11]Addoms, R.B. and Spaid, F.W., "Aerodynamic Design of High Performance Biplane Wings," McDonnell-Douglas Corporation Report, McDonnell-Douglas Corporation, St. Louis, Mo., 1975.

[12]Laitone, E.V., "Prandtl's Biplane Theory Applied to Canard and Tandem Aircraft," *Journal of Aircraft,* Vol. 17, April 1980, pp. 233-237.

[13]Kroo, I.M., "Minimum Induced Drag of Canard Configurations," *Journal of Aircraft,* Vol. 19, Sept. 1982, pp. 792-794.

[14]Butler, G.F., "Effect of Downwash on the Induced Drag of Canard-Wing Combinations," AIAA Paper 72-221, 1972.

[15]Liebeck, R.H., "Theoretical Studies on the Aerodynamics of Slat Airfoil Combinations," AIAA Paper 72-221, 1972.

[16]Lissaman, P.B.S. and O'Pray, J.E., "Slat Design by a Semi-Inverse Technique," AIAA Paper 71-11, 1971.

[17]Smith, A.M.O., "High Lift Aerodynamics-37th Wright Brothers Lecture," 13th AIAA Aerospace Sciences Meeting, Pasadena, Calif., 1975.

[18]Rokhsaz, K., "Analytical Investigation of the Aerodynamic Characteristics of Dual Wing Systems," Thesis, University of Missouri, Rolla, Mo., 1980.

[19]McGhee, R.J., "Wind Tunnel Results for a 13-Percent-Thick Medium Speed Airfoil Section," (NASA TM in publication).

[20]Sommers, D.M., "Design and Experimental Results for a Flapped Natural-Laminar-Flow Airfoil for General Aviation Applications," NASA TR-1865, June 1981.

[21]Thwaites, B., "Approximate Calculation of the Laminar Boundary Layer," Aeronautical Quarterly, Vol. 1, pp. 245-280, 1949.

[22]Michel, R., "Etude de la Transition sur les Profiles d' Aile; Establissement d'un Critere de Determination de Point de Transition

Downloaded by ISAE on October 25, 2021 | http://arc.aiaa.org | DOI: 10.2514/3.48234

et Calcul de la Trainee de Profile Incompressible," ONERA Rept. 1/1578A, 1951.

[23]Cebeci, T. and Bradshaw, P., *Momentum Transfer in Boundary Layers,* Hemisphere Publishing Corp., Washington, 1977, pp. 192-194.

[24]Cebeci, T. and Smith, A.M.O., "Calculation of Profile Drag of Airfoils at Low Mach Numbers," *Journal of Aircraft,* Vol. 5, Nov.-Dec. 1968, pp. 535-542.

[25]Beasley, J.A., "Calculation of the Laminar Boundary Layer and Prediction of Transition on a Sheared Wing," R.A.E. Rept. 3787, Oct. 1973.

[26]Rokhsaz, K. and Selberg, B.P., "Disadvantages of Thin Airfoil Formulations for Closely Coupled Airfoils," *Journal of Aircraft,* Vol. 20, June 1983, pp. 574-576.

[27]Rokhsaz, K., Internal correspondence, University of Missouri, 1981.

[28]Tulinius, J., "Unified Subsonic, Transonic, and Supersonic NAR Vortex Lattice," North American Rockwell, Los Angeles, Calif., TFD-72-523, 1972.

[29]Paulson, J.W., "Application of Vortex Lattice Theory to Preliminary Aerodynamic Design," NASA TN-D-8236 1976.

[30]Holmes, B.J. and Croom, C.C., "Aerodynamic Design Data for a Cruise-Matched High Performance Single Engine Airplane," SAE Paper 810625, 1981.

[31]Benstein, E.H. and Smith, R., "Advanced General Aviation Turbine Engine (GATE) Study," NASA CR-159624, 1979.

[32]Whitcomb, R.T., "A Design Approach and Selected Wind-Tunnel Results at High Subsonic Speeds for Wing-Tip Mounted Winglets," NASA TN D-8260, 1976.

[33]Nicolai, L.M., *Fundamentals of Aircraft Design,* METS, Inc., San Jose, Calif., 1975, pp. 5.1-5.24 and 20.1-20.24.

[34]Torenbeek, E., *Synthesis of Subsonic Airplane Design,* Delft University Press, Delft, Holland, 1976, pp. 27-76, 263-302, 352.

[35]Torenbeek, E., "Prediction of Wing Group Weight for Preliminary Design," *Aircraft Engineering,* Vol. 43, July 1971, pp. 17-21.

[36]Hayes, B., Lopez, R., and Rhodes, M., "General Aviation Light Turbo-Powered Aircraft," Senior Design Project, University of Missouri, Rolla, 1980.

[37]Somnay, R.J., "Design of Dual Wing Structures," Thesis, University of Missouri, Rolla, Mo., 1983.

[38]Roskam, J., *Methods for Estimating Drag Polars of Subsonic Airplanes,* published by the author, Lawrence, Kan., 1971, p. 2.3.

[39]Hoerner, S.F., *Fluid Dynamic Drag,* published by the author, 1965, pp. 6.15-6.19.

[40]Crawford, D.R., *A Practical Guide to Airplane Performance and Design,* 1st Ed., Crawford Aviation, Torrance, Calif., 1979, p. 174.

[41]Roskam, J., *Methods for Estimating Stability and Control Derivatives of Conventional Subsonic Airplanes,* published by the author, Lawrence, Kan., 1971, pp. 2.1-12.2.

[42]Roskam, J., *Airplane Flight Dynamics and Automatic Flight Controls, Part I,* Roskam Aviation and Engineering Corp., Lawrence, Kansas, 1979, pp. 243-377.

Downloaded by ISAE on October 25, 2021 | http://arc.aiaa.org | DOI: 10.2514/3.48234

From the AIAA Progress in Astronautics and Aeronautics Series . . .

TRANSONIC AERODYNAMICS—v. 81

Edited by David Nixon, Nielsen Engineering & Research, Inc.

Forty years ago in the early 1940s the advent of high-performance military aircraft that could reach transonic speeds in a dive led to a concentration of research effort, experimental and theoretical, in transonic flow. For a variety of reasons, fundamental progress was slow until the availability of large computers in the late 1960s initiated the present resurgence of interest in the topic. Since that time, prediction methods have developed rapidly and, together with the impetus given by the fuel shortage and the high cost of fuel to the evolution of energy-efficient aircraft, have led to major advances in the understanding of the physical nature of transonic flow. In spite of this growth in knowledge, no book has appeared that treats the advances of the past decade, even in the limited field of steady-state flows. A major feature of the present book is the balance in presentation between theory and numerical analyses on the one hand and the case studies of application to practical aerodynamic design problems in the aviation industry on the other.

696 pp., 6×9, illus., $30.00 Mem., $55.00 List

TO ORDER WRITE: Publications Order Dept., AIAA, 1633 Broadway, New York, N.Y. 10019

This article has been cited by:

1. Fangzheng Chen, Jianqiao Yu, Yuesong Mei. 2018. Aerodynamic design optimization for low Reynolds tandem airfoil. *Proceedings of the Institution of Mechanical Engineers, Part G: Journal of Aerospace Engineering* **232**:6, 1047-1062. [Crossref]
2. Nurhayyan H. Rosid, E. Irsyad Lukman, M. Ahmad Fadlillah, M. Agoes Moelyadi. 2018. Aerodynamic Characteristics of Tube-Launched Tandem Wing Unmanned Aerial Vehicle. *Journal of Physics: Conference Series* **1005**, 012015. [Crossref]
3. Liang Gao, Changle Li, Hongzhe Jin, Yanhe Zhu, Jie Zhao, Hegao Cai. 2017. Aerodynamic characteristics of a novel catapult launched morphing tandem-wing unmanned aerial vehicle. *Advances in Mechanical Engineering* **9**:2, 168781401769229. [Crossref]
4. Jian Chen, Pengwei Liu, Hongtao Xu, Liu Chen, Mo Yang, Liang Yang. 2017. A detailed investigation of a novel vertical axis Darrieus wind rotor with two sets of blades. *Journal of Renewable and Sustainable Energy* **9**:1, 013307. [Crossref]
5. Yong Feng Shang. 2013. Research on Unconventional Layouts of Aircraft. *Advanced Materials Research* **785-786**, 1189-1192. [Crossref]
6. . Clean Sheet Design 157-195. [Crossref]
7. G. Q. Zhang, S. C. M. Yu. 2012. Unsteady Aerodynamics of a Morphing Tandem-Wing Unmanned Aerial Vehicle. *Journal of Aircraft* **49**:5, 1315-1323. [Citation] [PDF] [PDF Plus]
8. Tracy Bagwill, Bruce Selberg, Tracy Bagwill, Bruce Selberg. Aerodynamic investigation of twist and cant angles for joined wing transport aircraft . [Citation] [PDF] [PDF Plus]
9. Joshua B. Jarvis, Bruce P. Selberg. Aerodynamic Investigation of Wing Tip Sails . [Crossref]
10. Daniel F. Scharpf, Thomas J. Mueller. 1992. Experimental study of a low Reynolds number tandem airfoil configuration. *Journal of Aircraft* **29**:2, 231-236. [Citation] [PDF] [PDF Plus]
11. Doug Blake, Bruce P. Selberg. Non Linear Induced Drag Study of Generically Cambered Closely Coupled Dual Wings . [Crossref]
12. Clarence Chenault, Bruce P. Selberg. CFD Calculations of Closely Coupled Scissor Wings-Inviscid, Viscous, and Vortex Lattice with Rollup Results . [Crossref]
13. DANIEL SCHARPF, THOMAS MUELLER. An experimental study of a closely coupled tandem wing configurationat low Reynolds numbers . [Citation] [PDF] [PDF Plus]
14. Kamran Rokhsaz, Bruce P. Selberg. 1989. Three-surface aircraft - Optimum vs typical. *Journal of Aircraft* **26**:8, 699-704. [Citation] [PDF] [PDF Plus]
15. Kamran Rokhsaz, Bruce P. Selberg. 1986. Dual-wing systems with decalage angle optimization. *Journal of Aircraft* **23**:5, 444-448. [Citation] [PDF] [PDF Plus]
16. Julian Wolkovitch. 1986. The joined wing - An overview. *Journal of Aircraft* **23**:3, 161-178. [Citation] [PDF] [PDF Plus]
17. B. SELBERG. Investigation of chord ratio, stagger, decalage angle, and flap angle for dual wing configurations . [Citation] [PDF] [PDF Plus]
18. K. ROKHSAZ, B. SELBERG. Dual and single wing design integration-optimized for decalage angle, R(e), and M(cr) . [Citation] [PDF] [PDF Plus]

Downloaded by ISAE on October 25, 2021 | http://arc.aiaa.org | DOI: 10.2514/3.48234